Available Online: 16 October 2026 DOI: 10.54254/3049-5458/2026.37658

An interpretable machine learning risk stratification model for the imaging burden of cerebral small vessel disease: integrating echocardiography, carotid ultrasound, and serological indicators

***Huilan Tan*[1], *Houwei Li*[1], *Chulin Deng*[1], *Sisi Liang*[1], *Jiafu Lan*[2,*]**

[1]Youjiang Medical University for Nationalities, Baise, China
[2]Affiliated Hospital of Youjiang Medical University for Nationalities, Baise, China

*Corresponding Author. Email: 18978600388@163.com

Abstract. This study enrolled 401 subjects, who were stratified according to the total imaging burden score of Cerebral Small Vessel Disease (CSVD) and divided into a training set (280 cases) and a validation set (121 cases) at a ratio of 7:3. Six variables—age, left ventricular posterior wall end-diastolic thickness, E/e′ ratio, maximum carotid plaque thickness, history of hypertension, and low-density lipoprotein cholesterol—were included, and Logistic regression, K-nearest neighbor, and partial least squares models were separately constructed. Performance was evaluated using the area under the receiver operating characteristic curve, sensitivity, specificity, and decision curve analysis. The results showed that the K-nearest neighbor model achieved the best performance in the validation set (AUC 0.869, accuracy 82.6%, sensitivity 65.0%, specificity 95.1%). SHAP analysis clarified the contribution of each feature, with E/e′ being the strongest predictor (mean absolute SHAP value 0.194), followed by maximum carotid plaque thickness and age (0.085 and 0.062, respectively). Decision curve analysis showed that the model yielded the greatest net benefit at a disease-risk threshold of 35%. With a specificity of 95.1%, the model performed prominently in risk stratification of CSVD patients, could effectively identify low-risk populations and reduce unnecessary imaging examinations, but its sensitivity was relatively low (65.0%), making it more suitable for clinical secondary diagnosis.

Keywords: cerebral small vessel disease, imaging burden, echocardiography, carotid ultrasound, machine learning

1. Introduction

Cerebral Small Vessel Disease (CSVD) is a chronic, progressive cerebrovascular disease caused by structural or functional abnormalities of the small arteries, arterioles, capillaries, and small veins within the brain, and it is a core pathological factor leading to stroke, cognitive decline, gait disturbance, and functional deterioration in the elderly population. In recent years, population aging has continued to intensify, and the disease burden

Copyright: © 2026 by the authors. Submitted for possible open access publication under the terms and conditions of the Creative Commons Attribution (CC BY) license (https://creativecommons.org/licenses/by/4.0/).

imposed by CSVD has kept rising, making it a key public health issue threatening the brain health of older adults [1, 2]. Cranial Magnetic Resonance Imaging (MRI) can clearly reveal the various imaging markers corresponding to CSVD, such as white matter hyperintensity, lacunar infarction, cerebral microbleeds, and enlarged perivascular spaces. Current international guidelines have established a standardized imaging assessment framework and proposed the use of the total CSVD score to quantify the overall damage burden of cerebral small vessels [3, 4].

Numerous studies have amply demonstrated that an elevated imaging burden of CSVD is associated with increased risks of ischemic stroke, intracerebral hemorrhage, cognitive decline, and all-cause mortality. An excessively high CSVD burden not only reflects the severity of cerebral microcirculatory injury but can also serve as a key predictor for the occurrence of subsequent cerebrovascular events; therefore, early identification of CSVD medium-to-high-burden populations and implementation of precise risk stratification carry high clinical practical value [3, 5]. However, current assessment of CSVD burden mostly relies on MRI as the principal modality, yet MRI has limitations such as relatively high examination cost, demanding hardware requirements, and the inability to examine some patients who have contraindications, which creates many obstacles to its application in large-sample population screening and primary-care settings. Precisely for this reason, the development of alternative assessment methods that are simple to perform, non-invasive, and suitable for widespread use has become one of the current research hotspots in the CSVD field [6, 7].

CSVD shares pathophysiological mechanisms with systemic vascular aging and arteriosclerosis. In recent years, the "heart–brain axis" theory has attracted growing attention; this theory holds that disturbances in cardiac structure and function, increased arterial stiffness, and vascular endothelial injury can induce cerebral small-vessel damage through pathways such as hemodynamic disturbance, inflammatory response, and oxidative stress [8]. Therefore, some related indicators of the cardiovascular system may become key observation entry points for judging the health status of cerebral small vessels. Echocardiography can non-invasively assess the structural and functional state of the heart and identify subclinical cardiovascular lesions such as left ventricular hypertrophy, left atrial enlargement, and diastolic dysfunction. Existing studies have shown that cardiac structural remodeling and functional abnormalities are related to white matter damage, cognitive decline, and cerebral small-vessel disease, which also implies that echocardiographic parameters can signal the risk of occult cerebrovascular injury [9, 10]. In addition, carotid ultrasound can evaluate the progression of systemic atherosclerosis and vascular function, with detected indicators including carotid intima-media thickness, plaque occurrence, and vascular stiffness-related parameters. Published studies have shown that the severity of carotid atherosclerosis is independently correlated with white matter hyperintensity, lacunar infarction, and the total CSVD burden score, indicating that carotid ultrasound indicators have potential predictive value for cerebral small-vessel injury [11].

Existing studies have separately confirmed that echocardiographic or carotid ultrasound indicators are associated with CSVD, yet relying solely on the detection indicators of a single system cannot comprehensively present the complex interactions between the cardiovascular and cerebrovascular systems. In view of this research limitation, the present study introduces the "heart–neck axis" theoretical framework, conducts a joint analysis of echocardiographic and carotid ultrasound parameters, and thereby evaluates the imaging burden level of CSVD from the perspective of overall vascular function. Moreover, the occurrence and progression of CSVD result from the combined action of multiple pathways including chronic inflammatory response, metabolic disturbance, coagulation dysfunction, and endothelial injury. Serological indicators can provide an independent biological reference basis for such pathological processes [12, 13]. Based on this, the "heart–neck axis" comprehensive assessment model—which integrates echocardiographic indicators reflecting left ventricular diastolic function and structural changes, carotid ultrasound indicators

reflecting the burden of large-vessel atherosclerosis, and serological markers indicating systemic metabolic and inflammatory status—may offer a new and feasible pathway for the assessment of overall vascular function in relation to the severity of cerebral small-vessel injury.

Machine learning is increasingly widely applied in the field of medical prediction. Compared with traditional statistical methods, its advantage lies in handling the nonlinear relationships among multidimensional variables and improving prediction accuracy through feature selection and pattern recognition. This technology has achieved good results in stroke risk assessment, brain image analysis, and prognostic evaluation of neurodegenerative diseases [14, 15]. The insufficient interpretability of complex machine learning models constrains their clinical application, and advances in explainable artificial intelligence have provided a solution for this; the SHAP algorithm can quantify the contribution of each variable to the model output and enhance model transparency and clinical readability [16]. This method takes the Shapley value under the game-theoretic framework as its core theoretical basis, and by solving the average marginal contribution of each feature to the model prediction, it achieves a quantitative measurement of the relative importance of each feature [17]. Compared with traditional feature-importance assessment methods, SHAP can capture nonlinear associations and interaction effects among variables, providing more scientific support for clinical decision-making. Integrating SHAP into the machine learning model-building process can identify the key features affecting the imaging burden of CSVD and enhance the clinical utility of the model.

This study adopted a three-tier progressive feature screening strategy: (1) combining published conclusions and univariate analysis to preliminarily screen candidate variables related to CSVD burden from more than 20 indicators; (2) applying variance inflation factor tests to exclude collinear indicators and ensure model stability; (3) integrating clinical value and statistical significance to finally include 6 independent predictor variables. These six variables span three dimensions: the cardiac dimension (left ventricular posterior wall end-diastolic thickness, E/e′), the vascular dimension (the sum of maximum thickness of bilateral carotid plaques), and the risk-factor dimension (age, history of hypertension, dyslipidemia), forming an integrated "heart–neck axis" assessment framework.

This study integrates echocardiography, carotid ultrasound, and serological indicators, and applies machine learning to establish a risk stratification model for the imaging burden of CSVD. Receiver operating characteristic curves, area under the curve, calibration curves, decision curve analysis, and the SHAP method are used for multidimensional performance evaluation, providing a quantitative basis for the early non-invasive screening and precise risk management of CSVD.

2. Materials and methods

2.1. Ethical statement and informed consent

This retrospective study was approved by the Institutional Review Board of our hospital and conducted in accordance with the ethical principles of the Declaration of Helsinki; given that this study was retrospective, the ethics committee waived the requirement for obtaining individual informed consent.

2.2. Study population

This study retrospectively enrolled 401 patients who visited the Affiliated Hospital of Youjiang Medical University for Nationalities from January 2023 to May 2026, were diagnosed with CSVD, and completed MRI, echocardiography, carotid ultrasound, and fasting blood tests. Inclusion criteria: 1) patients diagnosed with CSVD by MRI; 2) cranial MRI images showing at least one of the five imaging features—recent subcortical small infarction, lacune, white matter hyperintensity, cerebral microbleed, and enlarged

perivascular space—with image quality meeting the scoring criteria; 3) completion of transthoracic echocardiography and carotid ultrasound examinations; 4) complete serological indicator data. Exclusion criteria: 1) concomitant large-area cerebral infarction, intracerebral hemorrhage, craniocerebral trauma, intracranial infection, or other neurological diseases that might affect imaging evaluation of CSVD; 2) concomitant severe coronary heart disease, valvular heart disease, cardiomyopathy, decompensated heart failure, or severe arrhythmia and other diseases that markedly affect cardiac structure and function; 3) prior carotid artery surgery or interventional treatment, or anatomical abnormalities affecting carotid ultrasound measurement; 4) concomitant severe hepatorenal insufficiency, malignant tumor, or active infection; 5) presence of contraindications to cranial MRI examination, or image quality not meeting assessment requirements; 6) incomplete medical record data.

2.3. Collection of MRI, echocardiography, carotid ultrasound, and serological data

Cranial MRI scans of the subjects were performed using a 3.0 Tesla Signa HD superconducting MRI scanner from GE (USA). The scanning sequences included T1-weighted imaging, T2-weighted imaging, fluid-attenuated inversion recovery, diffusion-weighted imaging, and susceptibility-weighted imaging. The basic characteristics (such as age, sex, BMI, and hypertension), ultrasound data (such as left ventricular posterior wall end-diastolic thickness, mean carotid intima-media thickness, and the sum of maximum carotid plaque thickness), and serological indicators (total cholesterol, low-density lipoprotein, high-density lipoprotein, etc.) were collected.

2.4. Total CSVD imaging burden score

All MRI images were independently assessed by two researchers according to standardized guidelines [3, 4]. The sequential scoring system described in references [3, 4] (actual score range 0–4) was used to quantitatively grade the overall CSVD burden. The system covers four MRI markers: cerebral lacune (≥ 1) scores 1 point; deep white matter hyperintensity with early confluence (Fazekas 2 or 3) or periventricular white matter hyperintensity irregularly invading deep white matter (Fazekas 3) scores 1 point; moderate-to-severe enlarged perivascular spaces in the basal ganglia region scores 1 point; and cerebral microbleed (≥ 1) scores 1 point. Disagreements were resolved by consensus between the two researchers. According to the classification threshold of previous studies [12], those with a total score of 0–1 were defined as the Low CSVD burden group (CSVD-L), and those with a total score of 2–4 were assigned to the Medium-to-High CSVD burden group (CSVD-MH).

2.5. Statistical analysis

Statistical analysis and machine learning modeling were performed using R software (version 4.0.0). After the Shapiro–Wilk test for continuous variables, data conforming to a normal distribution were expressed as mean ± standard deviation and compared using the independent-samples t-test, while non-normally distributed data were expressed as median (interquartile range) and compared using the Mann–Whitney U test. Categorical data were analyzed using the χ^2 test or Fisher's exact test, with bilateral $p < 0.05$ considered statistically significant. The 401 patients were divided into a training set (280 cases) and a validation set (121 cases) at a 7:3 ratio, with stratified sampling used to ensure consistent burden distribution across groups. Because medium-to-high-burden patients accounted for 24.2%, the training set used SMOTE oversampling (multiplier $k = 3$) to address class imbalance, while the validation set retained the original distribution to objectively reflect model performance. Univariate analysis screened variables with $p < 0.05$, which entered stepwise Logistic regression (AIC criterion, forward method, inclusion $p < 0.05$, exclusion $p > 0.10$) to determine

independent predictor variables. Multicollinearity was examined by calculating the Variance Inflation Factor (VIF), features were processed by Z-score standardization, and the standardization parameters were computed solely from the training set and then applied to the validation set to avoid data leakage. This study constructed three types of models—Logistic regression, K-nearest neighbor (K values 3–15, optimized by 5-fold cross-validation, Euclidean distance, distance-inverse weighting), and partial least squares regression. Model performance was evaluated through ROC curves (AUC and its 95% confidence interval), calibration curves (Brier score), and Decision Curve Analysis (DCA), and indicators such as sensitivity, specificity, and accuracy were calculated; the optimal model was selected after comprehensive comparison. The SHAP method was used for interpretability analysis of the optimal model, and the mean absolute SHAP value of each feature was calculated to quantify its contribution to the prediction outcome; the direction and relative importance of each variable's influence on the medium-to-high CSVD burden risk were displayed through feature importance plots and SHAP beeswarm plots.

3. Results

3.1. Comparison of baseline characteristics and imaging burden grouping in CSVD patients

A total of 401 CSVD patients were enrolled and all study subjects were divided into a low-burden group and a medium-to-high-burden group, with 264 cases in the low-burden group and 137 cases in the medium-to-high-burden group. The age, sex, BMI, and main clinical indicators of the two groups are shown in Table 1. No significant differences were found between the two groups in sex, BMI, history of diabetes, or history of hyperlipidemia. The prevalence of hypertension and age in the medium-to-high-burden group were both significantly higher than those in the low-burden group ($p < 0.05$). Among the serological indicators, high-density lipoprotein cholesterol, triglycerides, platelets, monocytes, neutrophils, and SIRI levels showed no differences between the two groups; the low-density lipoprotein cholesterol, total cholesterol, glycated hemoglobin, and lymphocyte count in the medium-to-high-burden group were significantly higher than those in the low-burden group ($p < 0.05$).

Table 1. Comparison of baseline data between CSVD imaging burden groups

Baseline indicators	Low-burden group ($N = 264$)	Medium-to-high-burden group ($N = 137$)	p value
Age (years, mean ± SD)	63.44 ± 8.70	68.09 ± 9.19	< 0.001
Male, *n* (%)	174 (65.9%)	90 (65.7%)	0.966
BMI (kg/m², M[P25, P75])	24.18 (21.87, 26.62)	23.44 (21.39, 26.11)	0.208
Hypertension, *n* (%)	169 (64.0%)	111 (81.0%)	< 0.001
Diabetes, *n* (%)	199 (75.4%)	73 (53.3%)	< 0.001
Hyperlipidemia, *n* (%)	232 (87.9%)	118 (86.1%)	0.618
Glycated hemoglobin (HbA1c), M[P25, P75]	7.80 (5.90, 10.33)	6.40 (5.70, 8.90)	0.003
TC (mmol/L, M[P25, P75])	4.97 (3.98, 5.97)	4.57 (3.66, 5.28)	0.002
LDL-C (mmol/L, M[P25, P75])	3.02 (2.20, 3.74)	2.70 (2.13, 3.40)	0.020
HDL-C (mmol/L, M[P25, P75])	1.08 (0.90, 1.33)	1.06 (0.88, 1.32)	0.388
TG (mmol/L, M[P25, P75])	1.49 (0.99, 2.32)	1.44 (0.93, 2.31)	0.451

Table 1. Continued

PLT (×10⁹/L, M[P25, P75])	247.00 (209.50, 292.25)	246.00 (196.00, 308.00)	0.945
Monocyte count (×10⁹/L, M[P25, P75])	0.51 (0.39, 0.66)	0.52 (0.41, 0.67)	0.757
Neutrophil count (×10⁹/L, M[P25, P75])	4.50 (3.61, 5.94)	4.40 (3.57, 5.87)	0.510
Lymphocyte count (×10⁹/L, M[P25, P75])	1.71 (1.37, 2.19)	1.57 (1.21, 1.97)	0.013
SIRI, M[P25, P75]	1.29 (0.85, 2.03)	1.51 (0.86, 2.46)	0.250

Note: Among the test statistics, age corresponds to the t value; skewed continuous variables correspond to the Z value; and categorical variables correspond to the χ^2 value. $p < 0.05$ indicates a statistically significant difference.

3.2. Comparison of echocardiographic and carotid ultrasound indicators between imaging burden groups

Table 2. Comparison of echocardiographic and carotid ultrasound indicators between CSVD imaging burden groups

Variable	Low-burden group (n = 264)	Medium-to-high-burden group (n = 137)	p value
LAD	31.00 (29.00, 34.00)	32.00 (29.00, 34.00)	0.840
IVS	9.00 (8.00, 10.00)	9.00 (9.00, 10.00)	0.442
LVPW	9.00 (8.00, 10.00)	9.00 (9.00, 10.00)	0.014
LVESD	28.00 (25.00, 31.00)	28.00 (26.00, 31.00)	0.503
LVEDD	45.00 (42.00, 49.00)	46.00 (41.00, 49.00)	0.789
EF	0.67 (0.61, 0.73)	0.67 (0.61, 0.72)	0.472
MPA	22.00 (20.00, 24.00)	22.00 (20.00, 24.00)	0.331
RWT	0.41 (0.37, 0.46)	0.43 (0.38, 0.47)	0.046
LVMI	87.51 (72.17, 105.21)	89.94 (76.75, 109.55)	0.166
E/e′	9.90 (8.00, 11.80)	16.00 (11.00, 19.10)	<0.001
CIMT	0.75 (0.70, 0.85)	0.80 (0.70, 1.00)	<0.001
CPTsum	2.60 (1.60, 4.10)	5.60 (4.60, 6.90)	<0.001
LDL-C	3.02 (2.20, 3.74)	2.70 (2.13, 3.40)	0.020

Note: Variables are expressed as M (P25, P75). The Mann–Whitney U test was used. $p < 0.05$ indicates a statistically significant difference.

The echocardiographic and carotid ultrasound parameters of the two groups were further compared according to the above grouping. The results showed that the differences in LAD, IVS, ESD, EDD, EF, MPA, LVM, and LVMI between the two groups were all statistically insignificant ($p > 0.05$). Compared with the low-burden group, the medium-to-high-burden group had higher LVPW, RWT, and E/e′ levels and lower interventricular septum e′, lateral wall e′, and mean e′ levels, and all these differences were statistically significant ($p < 0.05$). Regarding carotid ultrasound indicators, the CIMT and CPTsum in the medium-to-high-burden group were both higher than those in the low-burden group, and the difference was statistically

significant ($p < 0.001$). The above results suggest that an elevated CSVD imaging burden may be related to left ventricular diastolic dysfunction, left ventricular structural changes, and increased carotid atherosclerotic burden (see Table 2).

3.3. Candidate variable screening and prediction model construction

Based on the comparison of clinical characteristics, laboratory indicators, and ultrasound indicators between the two patient groups in the training set, and considering clinical significance and variable correlation, six features—age, LVPWd, E/e′, CPTsum, hypertension, and LDL-C—were included to build the machine learning model. With high CSVD imaging burden as the positive outcome, Logistic regression, K-nearest neighbor, and partial least squares regression models were respectively constructed. All models completed fitting and parameter optimization on the training set.

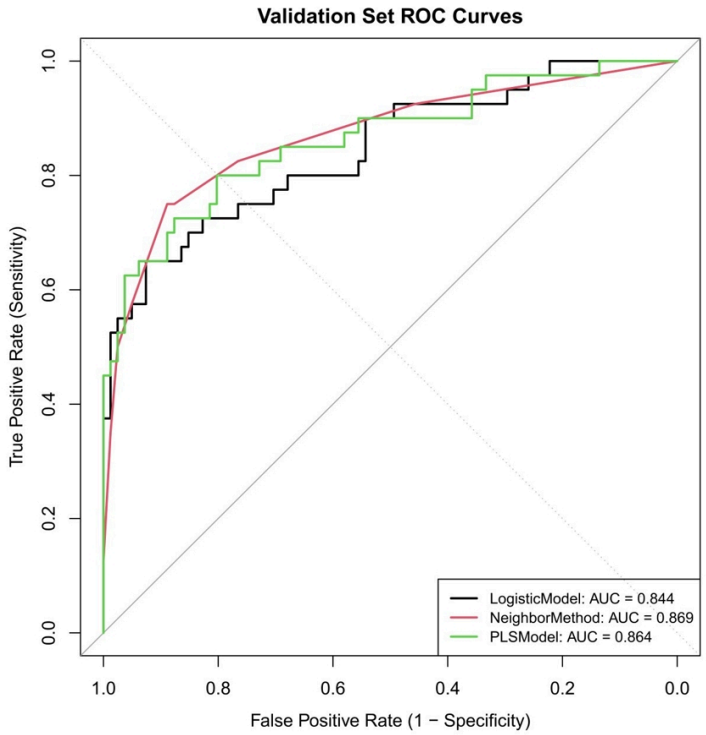


Figure 1. ROC curves of three machine learning models in the validation set

Note: The horizontal axis is the false positive rate (1 − specificity), ranging from 0 to 1.0; the vertical axis is the true positive rate (sensitivity), ranging from 0 to 1.0. The dashed line represents the reference line of a random classifier (AUC = 0.5). The black line represents the Logistic regression model (AUC = 0.844), the red line represents the K-nearest neighbor model (AUC = 0.869), and the green line represents the partial least squares model (AUC = 0.864).

In the validation set, the K-nearest neighbor model showed the best overall performance (AUC 0.869, accuracy 82.64%, specificity 95.06%, positive predictive value 85.19%), the strongest generalization stability (training/validation AUC difference only 0.027), and good calibration curve fit (Brier score 0.121 vs 0.125). The Logistic regression model had higher sensitivity (70.00%), and the F1 score and Youden index of the partial least squares model were between the two, as shown in Figures 1 and 2. Decision curve analysis showed that the K-nearest neighbor model maintained positive net benefit over a wider threshold range and outperformed both the treat-all and treat-none strategies, as shown in Figure 3. SHAP feature importance analysis indicated that E/e′ (mean absolute SHAP value 0.194) was the core driving factor of the model, showing a nonlinear threshold characteristic (SHAP value increased significantly when E/e′ ≥ 16), followed by CPTsum (0.085) and age (0.062), while the contributions of LDL-C, LVPWd, and hypertension history were relatively low (≤ 0.024), as shown in Figure 4. Integrating all indicators, the K-nearest neighbor model is most suitable as a primary diagnostic tool and has good clinical application value.

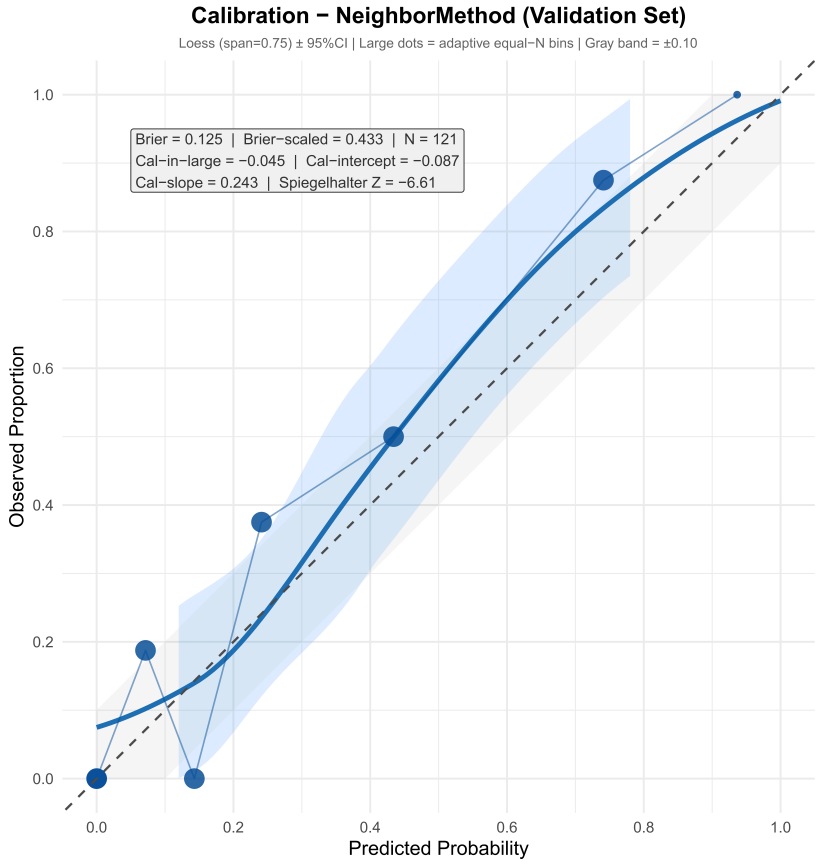


Figure 2. Calibration curve of the K-nearest neighbor model in the validation set

Note: The horizontal axis is the predicted probability (0–1.0) and the vertical axis is the observed proportion (0–1.0). The dashed line is the perfect calibration line, the blue solid line is the Lowess-smoothed calibration curve, the blue solid dots are the observed proportions after adaptive equal-width binning, and the light blue shaded band is the 95% CI range of ± 0.10.

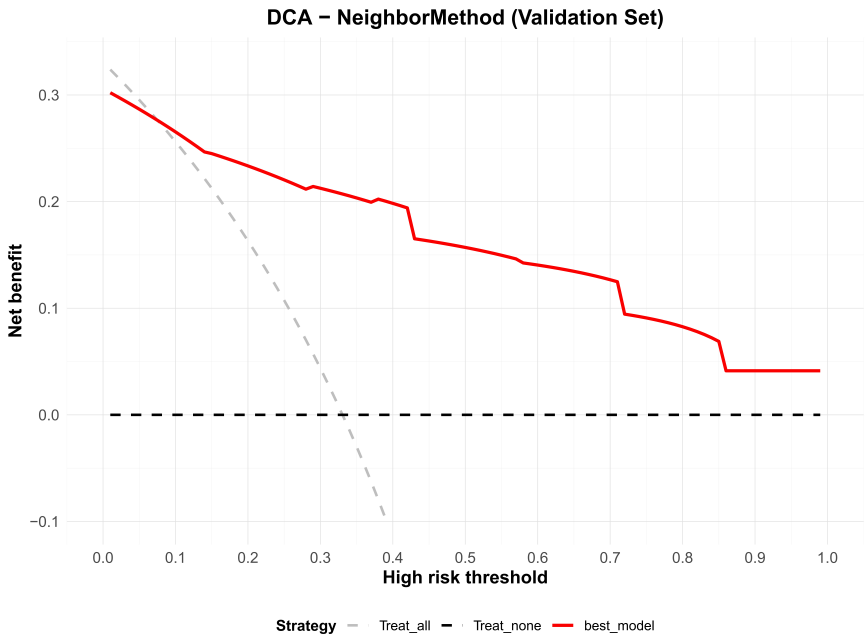


Figure 3. Decision curve analysis (DCA) of the K-nearest neighbor model in the validation set

Note: Decision curve analysis of the K-nearest neighbor model in the validation set. The horizontal axis is the high-risk threshold (0–1.0) and the vertical axis is the net benefit (−0.1 to 0.35). The gray dashed line (Treat_all), the black dashed line (Treat_none), and the red solid line (best_model) represent the treat-all, treat-none, and model strategies, respectively.

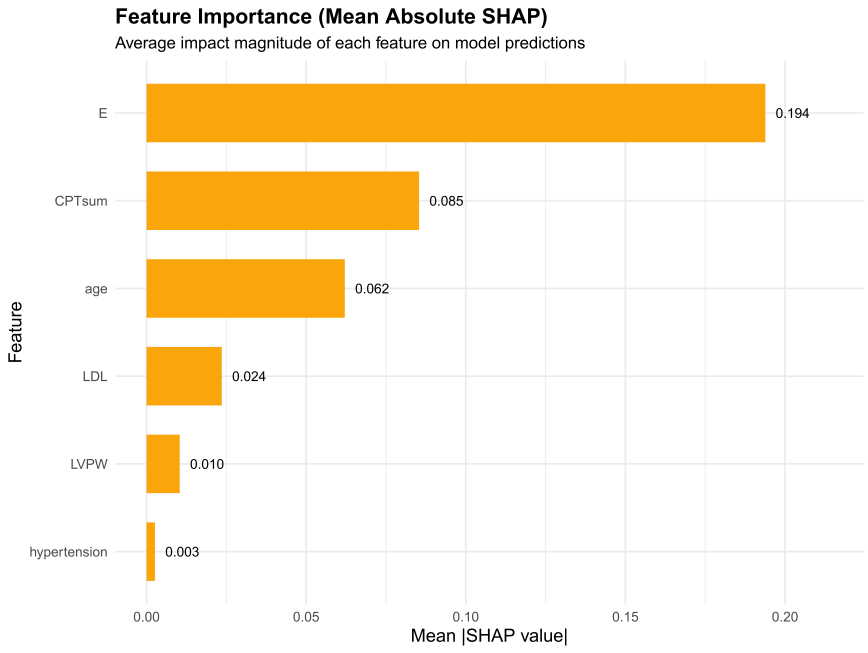


Figure 4. Feature importance ranking of the K-nearest neighbor model (mean absolute SHAP value)

Note: The chart shows the average magnitude of influence of each input feature on the K-nearest neighbor model's prediction of medium-to-high CSVD burden patients. The horizontal axis represents the mean absolute SHAP value (Mean|SHAP value|), reflecting the average magnitude of each feature's influence on the model output across all predictions, ranging from 0 to 0.20.

The vertical axis lists the six input features: E (mitral inflow velocity ratio), CPTsum (Total Carotid Plaque burden), age, LDL (Low-Density Lipoprotein cholesterol), LVPW (Left Ventricular Posterior Wall thickness), and hypertension. The bar length is proportional to feature importance.

4. Discussion

4.1. Major findings

This study established a K-nearest neighbor machine learning model based on integrated "heart–neck axis" assessment for risk stratification of CSVD imaging burden. The validation set results showed that the model achieved an AUC of 0.869 (95% CI: 0.795–0.942), an accuracy of 82.64%, a specificity of 95.06%, and a sensitivity of 65.00%. Compared with Logistic regression (AUC 0.844, sensitivity 70.00%) and the partial least squares model (AUC 0.864), the K-nearest neighbor model had the best generalization stability (training/validation AUC difference only 0.027) and good calibration performance (Brier score 0.121 vs 0.125). SHAP feature importance analysis showed that E/e′ (mean absolute SHAP value 0.194) was the core driving factor, exhibiting a nonlinear threshold characteristic (SHAP value increased significantly when E/e′ ≥ 16), followed by CPTsum (0.085) and age (0.062), while the contributions of LDL-C, LVPWd, and hypertension history were relatively limited (≤ 0.024). Decision curve analysis showed that the model maintained positive net benefit within the threshold probability interval of 0.15–0.65, outperforming both the treat-all and treat-none strategies.

4.2. Interpretation based on existing evidence

Left ventricular diastolic dysfunction is a key pathological driver of CSVD. Previous studies have confirmed that left ventricular diastolic dysfunction is independently associated with white matter hyperintensity burden and cognitive decline [9], and that elevated left ventricular mass index is independently associated with the total CSVD burden score [10]. The nonlinear threshold effect of E/e′ found in this study suggests that only when diastolic dysfunction develops to a certain degree does it significantly increase the risk of CSVD. The possible mechanism is that left ventricular diastolic dysfunction leads to reduced cardiac output and decreased cerebral perfusion pressure, aggravates cerebral small-vessel endothelial cell injury, disrupts the blood–brain barrier structure, and ultimately causes cerebral microcirculatory homeostasis imbalance and white matter ischemic damage [18]. Carotid atherosclerotic burden shows a stable positive correlation with CSVD [19]; the mechanisms include: plaques releasing pro-inflammatory substances that aggravate systemic inflammatory response and impair vascular endothelial function [20]; carotid arteriosclerosis increasing pulse wave velocity and pulse pressure, raising cerebrovascular pulse stress load and disrupting cerebral capillary endothelial integrity [21]; and carotid atherosclerosis, as a marker of systemic microvascular dysfunction, directly damaging cerebral small vessels. The positive correlation trend of age reflects the cumulative effect of vascular aging, and the potential interaction between age and E/e′ indicates that the amplification effect of diastolic dysfunction on CSVD risk is more pronounced in the elderly population, consistent with the pathological mechanism of "accumulated and superimposed multi-dimensional vascular injury". In contrast, the marginal contributions of LDL-C, LVPWd, and hypertension are affected by multiple factors: the study has a healthy selection bias (the medium-to-high-burden group had a lower prevalence of diabetes), the widespread clinical use of antihypertensive drugs may weaken the predictive value of blood pressure itself [22], the SHAP analysis reflects the relative contribution within a model that already includes strong predictors such as E/e′ rather than a biological independent effect [23], and the effect of hypertension on

CSVD may have a nonlinear threshold characteristic, which the binary variable setting failed to fully capture the influence of blood pressure management level and fluctuation characteristics [24].

4.3. Clinical and research significance

This study innovatively and systematically integrates echocardiography, carotid ultrasound, and serum biomarkers, breaking through the limitations of single-discipline detection. Compared with the problems of MRI such as high cost, strong equipment dependence, and difficulty in primary-care promotion, the "heart–neck axis" integrated model has the advantages of convenient operation, low cost, and easy popularization. The high specificity of the K-nearest neighbor model (95.06%) makes it suitable for large-scale population screening (such as community stroke prevention and control) and can effectively reduce unnecessary follow-up examinations; the high sensitivity of the Logistic regression model (70.00%) makes it suitable for risk stratification of symptomatic patients and can avoid missed diagnosis of high-risk patients. The Youden indices of the two models are close (0.526 vs 0.527), suggesting that the choice in clinical application should be based on the specific scenario. This model provides a new idea for the non-invasive risk screening and precise management of CSVD and helps achieve early detection, stratified intervention, and individualized treatment. The nonlinear threshold characteristic of E/e′ revealed by SHAP analysis provides a quantitative basis for determining clinical intervention thresholds. In the future, novel lipid markers such as oxidized low-density lipoprotein and lipoprotein-associated phospholipase A2, as well as precise blood pressure indicators such as 24-hour ambulatory blood pressure and blood pressure variability, could be considered for inclusion to further optimize the predictive performance of the model.

4.4. Study limitations

This study has the following limitations: (1) In terms of study design, the single-center retrospective cohort has selection bias; all enrolled subjects were already diagnosed patients, and high-risk but undiagnosed community populations were not included, which affects the model's generalizability. The sample size was relatively small (280 in the training set and 121 in the validation set), and the proportion of medium-to-high-burden patients was low (34.6% and 33.1%), which may lead to insufficient learning of minority-class features by the model and reduce the prediction accuracy for high-burden patients. (2) In terms of information dimension, the cross-sectional design only reflects the disease burden at a single time point and cannot verify the model's predictive performance for long-term progression trends. The serological indicators only included routine test items and did not include novel biomarkers and inflammatory factors such as phosphorylated tau protein, β-amyloid, glial fibrillary acidic protein, and C-reactive protein, which may miss key biological clues and weaken the biological interpretability. (3) The insufficient calibration effect can be attributed to: heterogeneity of baseline characteristics between the training and validation populations; the K-nearest neighbor non-parametric algorithm tending to cause fluctuation in probability estimation of boundary samples; and the single-center data having population selection bias and acquisition bias. It is recommended that subsequent multi-center prospective external validation studies be conducted to evaluate the model's generalization performance and calibration efficacy in heterogeneous populations [25], and that longitudinal follow-up data (6-month, 1-year, and 3-year MRI re-examinations) be included for dynamic validation.

5. Conclusion

By integrating echocardiography, carotid ultrasound, and serological indicators, this study established an interpretable prediction model for the imaging burden of CSVD. The K-nearest neighbor model performed

well in the validation set (AUC 0.869, specificity 95.06%, positive predictive value 85.19%). SHAP analysis confirmed E/e′, CPTsum, and age as the core predictors, among which E/e′ exhibited a nonlinear threshold effect, providing quantitative support for the mechanistic role of left ventricular diastolic function in the pathology of CSVD. However, the sensitivity was only 65.00%, and the calibration performance requires validation by an independent cohort. In the future, iterative optimization can be achieved through multi-center prospective design, inclusion of novel biomarkers (phosphorylated tau, β-amyloid, etc.), and optimization of classification thresholds, thereby providing a more reliable objective basis for the non-invasive screening, risk stratification, and individualized prevention and control of CSVD.

References

[1] Litak, J., Mazurek, M., Kulesza, B., Szmygin, P., Litak, J., & Kamieniak, P. (2020). Cerebral small vessel disease. *International Journal of Molecular Sciences, 21*(24), Article 9729. https://doi.org/10.3390/ijms21249729

[2] Ter Telgte, A., van Leijsen, E. M. C., Wiegertjes, K., Klijn, C. J. M., Tuladhar, A. M., & de Leeuw, F. E. (2018). Cerebral small vessel disease: From a focal to a global perspective. *Nature Reviews Neurology, 14*(7), 387–398. https://doi.org/10.1038/s41582-018-0014-y

[3] Duering, M., Biessels, G. J., Brodtmann, A., Chen, C., Cordonnier, C., de Leeuw, F. E., Debette, S., Frayne, R., Jouvent, E., Rost, N. S., Ter Telgte, A., Al-Shahi Salman, R., Backes, W. H., Bae, H. J., Brown, R., Chabriat, H., De Luca, A., deCarli, C., Dewenter, A., … Dichgans, M. (2023). Neuroimaging standards for research into small vessel disease—Advances since 2013. *The Lancet Neurology, 22*(7), 602–618. https://doi.org/10.1016/S1474-4422(23)00131-X

[4] Wardlaw, J. M., Smith, E. E., Biessels, G. J., Cordonnier, C., Fazekas, F., Frayne, R., Lindley, R. I., O'Brien, J. T., Barkhof, F., Benavente, O. R., Black, S. E., Brayne, C., Breteler, M., Chabriat, H., DeCarli, C., de Leeuw, F. E., Doubal, F., Duering, M., Fox, N. C., … Dichgans, M. (2013). Neuroimaging standards for research into small vessel disease and its contribution to ageing and neurodegeneration. *The Lancet Neurology, 12*(8), 822–838. https://doi.org/10.1016/S1474-4422(13)70124-8

[5] Debette, S., Schilling, S., Duperron, M. G., Larsson, S. C., Markus, H. S., & Debette, S. (2019). Clinical significance of magnetic resonance imaging markers of vascular brain injury: A systematic review and meta-analysis. *JAMA Neurology, 76*(1), 81–94. https://doi.org/10.1001/jamaneurol.2018.3122

[6] Pantoni, L. (2010). Cerebral small vessel disease: From pathogenesis and clinical characteristics to therapeutic challenges. *The Lancet Neurology, 9*(7), 689–701. https://doi.org/10.1016/S1474-4422(10)70104-6

[7] Bordes, C., Sargurupremraj, M., Mishra, A., & Debette, S. (2022). Genetics of common cerebral small vessel disease. *Nature Reviews Neurology, 18*(2), 84–101. https://doi.org/10.1038/s41582-021-00592-8

[8] Mitchell, G. F. (2014). Arterial stiffness and hypertension. *Hypertension, 64*(1), 13–18. https://doi.org/10.1161/HYPERTENSIONAHA.114.00921

[9] Huang, J., Jali, V., Robert, C., & Chen, L. (2026). Association of left ventricular function with cerebral small vessel disease and cognition. *Journal of the American Heart Association, 15*(8), Article e045947. https://doi.org/10.1161/JAHA.125.045947

[10] Li, L., He, S., Xia, K., Wang, Y., Zhang, H., & Liu, J. (2026). A machine learning approach using echocardiographic and hematological parameters to classify cerebral small vessel disease burden. *Clinical Neurology and Neurosurgery, 266*, Article 109414. https://doi.org/10.1016/j.clineuro.2026.109414

[11] Xu, Y., Song, Y., Tang, T., Zhang, W., & Li, X. (2025). Correlation between neuroimaging scores and carotid artery ultrasound features in cerebral small vessel disease patients. *Cerebrovascular Diseases Extra, 15*(1), 93–101. https://doi.org/10.1159/000543355

[12] Rao, C., Zhu, L., Gu, T., Chen, Y., & Wang, H. (2026). Association of composite biomarkers with imaging burden in cerebral small vessel disease. *Lipids in Health and Disease, 25*(1), Article 47. https://doi.org/10.1186/s12944-025-02856-4

[13] Si, Z., Xiao, B., & Zhang, M. (2026). Metabolic dysregulation in cerebral small vessel disease: Pathogenesis and therapeutic targets. *Neuroscience, 599*, 170–184. https://doi.org/10.1016/j.neuroscience.2026.02.021

[14] Sheth, S. A., Giancardo, L., Colasurdo, M., Srinivasan, V. M., & Chen, P. R. (2023). Machine learning and acute stroke imaging. *Journal of NeuroInterventional Surgery, 15*(2), 195–199. https://doi.org/10.1136/neurintsurg-2021-018142

[15] Al Askar, A., Buchireddygari, D., Middi, B. V. S. R., Alsaadi, T., & Al-Khaled, M. (2025). The role of artificial intelligence and machine learning in the assessment, diagnosis, and prediction of cerebral small vessel disease. *Cureus, 17*(9), Article e93376. https://doi.org/10.7759/cureus.93376

[16] Guo, T., Wang, M., Wang, C., Zhang, Y., & Li, Q. (2025). Development and validation of an interpretable machine learning model for cerebral small vessel disease risk assessment. *International Journal of Medical Informatics, 204*, Article 106070. https://doi.org/10.1016/j.ijmedinf.2025.106070

[17] Lundberg, S. M., & Lee, S. I. (2017). A unified approach to interpreting model predictions. *Advances in Neural Information Processing Systems, 30*, 4765–4774.

[18] Rosenberg, G. A. (2017). Extracellular matrix inflammation in vascular cognitive impairment and dementia. *Clinical Science, 131*(6), 425–437. https://doi.org/10.1042/CS20160378

[19] Stoisavljevic, S., Zivkovic, M., & Rakic, A. (2024). Carotid artery stenosis is related to cerebral small vessel disease magnetic resonance imaging burden. *Heliyon, 10*(1), Article e23745. https://doi.org/10.1016/j.heliyon.2023.e23745

[20] Libby, P., Ridker, P. M., & Hansson, G. K. (2011). Progress and challenges in translating the biology of atherosclerosis. *Nature, 473*(7347), 317–325. https://doi.org/10.1038/nature10146

[21] Zhang, K., Jiang, Y., Wang, Y., & Xu, Y. (2020). Associations of arterial stiffness and carotid atherosclerosis with cerebral small vessel disease in a rural community-based population. *Journal of Atherosclerosis and Thrombosis, 27*(8), 783–793. https://doi.org/10.5551/jat.52780

[22] Zhu, X., Li, X., Wang, X., & Zhang, Y. (2026). Explainable XGBoost model and nomogram for risk factor identification and risk prediction in cerebral small vessel disease: A machine learning-based retrospective study. *Frontiers in Neurology, 17*, Article 1324567. https://doi.org/10.3389/fneur.2026.1324567

[23] Ribeiro, M. T., Singh, S., & Guestrin, C. (2016). "Why should I trust you?": Explaining the predictions of any classifier. *Proceedings of the 22nd ACM SIGKDD International Conference on Knowledge Discovery and Data Mining*, 1135–1144. https://doi.org/10.1145/2939672.2939778

[24] Mogi, M., & Horiuchi, M. (2011). Clinical interaction between brain and kidney in small vessel disease. *Cardiology Research and Practice, 2011*, Article 306918. https://doi.org/10.4061/2011/306918

[25] Des Jarlais, D. C., Lyles, C., & Crepaz, N. (2004). Transparent reporting of evaluations with nonrandomized designs (TREND). *Journal of Urban Health, 81*(2), 163–168. https://doi.org/10.1093/jurban/jth104